Hallway Gait Monitoring Using Novel Radar Signal Processing and Unsupervised Learning

Hajar Abedi, *Graduate Student Member, IEEE*, Jennifer Boger, *Member, IEEE*, Plinio P. Morita, *Member, IEEE*, Alexander Wong, *Senior Member, IEEE*, and George Shaker, *Senior Member, IEEE*

***Abstract*—We propose a novel corridor or hallway gait monitoring system based on radar signal processing, unsupervised learning, and a subject detection, association and tracking method. This paper proposes an algorithm that could be paired with any type of MIMO FMCW radar to capture human gait in a highly cluttered environment without needing radar antenna alteration. We validate algorithm functionality by capturing spatiotemporal gait values (e.g., speed, step points, step time, step length, and step count) of people walking in a long hallway. We show that our proposed algorithm yields an average absolute error for speed estimation between 0.0040 m/s to 0.0435 m/s. These preliminary results demonstrate the promising potential of our algorithm to accurately monitor gait in hallways, which increases opportunities for its applications in institutional and home environments.**

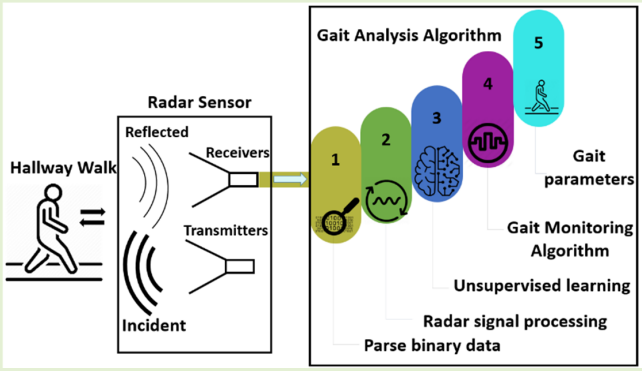

***Index Terms*—Contactless monitoring, doppler, frequency-modulated continuous-wave, multipath, multiple-input and multiple-output radar, gait analysis.**

I. Introduction

RADAR sensors appeal to healthcare applications, with potential benefits for older adults, healthcare systems, and the global economy [1]–[4]. One practical application is remote gait monitoring [5]–[10] as changes in gait can support detection and monitoring of changes in health. Extensive research and multiple longitudinal studies conducted on gait analysis [11]–[14] have shown that accurate, reliable knowledge of general gait characteristics at a given time, and even more importantly, over a period of time can enable detection and diagnosis of changes in mobility and cognition. Tracking gait can also support finding the best treatment options and ongoing management.

Several studies (e.g., [12], [15]) have concluded that a habitual or usual gait speed (i.e., walking at a normal speed on level ground) is considered a reliable and consistent clinical indicator. A person's walking speed in a clinical setting may not be an accurate and reliable representation of people's day-to-day gait because of their focus on walking and an awareness of the importance of the quality of their gait. Hence, it may negatively impact medical conclusions and recommendations. Thus diagnosis, follow-up, and treatment of pathologies from gait obtained in clinical settings may be based on inaccurate data. To obtain more accurate representation of day-to-day gait patterns, a quantification method of gait parameters in a naturalistic setting (e.g., one's home) is required. Gold standard systems such as the GaitRite mat system [16]–[18] and Vicon [19] can be expensive, difficult to operate, have limited coverage, and present challenges for deployment in real-world settings. Wearable sensors such as Opal sensor [20] and Physilog [21] could be used for day-to-day gait assessments; however, many people do not like using wearables or may not remember to wear them.

A radar-based sensor is a promising alternative to capture gait information during people's daily activities in their living environments over long periods as it is a relatively affordable, easy-to-use, non-invasive, and zero-effort system [9], [22]–[25].

Manuscript received 17 May 2022; revised 10 June 2022; accepted 11 June 2022. Date of publication 23 June 2022; date of current version 1 August 2022. This work was supported by Tandemlaunch Inc. The associate editor coordinating the review of this article and approving it for publication was Dr. Francesco Fioranelli. *(Corresponding author: Hajar Abedi.)*

This work involved human subjects or animals in its research. Approval of all ethical and experimental procedures and protocols was granted by the Local Board of the University of Waterloo under Application No. ORE # 31728.

Hajar Abedi, Jennifer Boger, and Alexander Wong are with the System Design Engineering Department, University of Waterloo, Waterloo, ON N2L 3G1, Canada (e-mail: habedifi@uwaterloo.ca; jboger@uwaterloo.ca; alexander.wong@uwaterloo.ca).

Plinio P. Morita is with the School of Public Health Sciences, University of Waterloo, Waterloo, ON N2L 3G1, Canada (e-mail: plinio.morita@uwaterloo.ca).

George Shaker is with the Electrical Engineering Department, University of Waterloo, Waterloo, ON N2L 3G1, Canada (e-mail: gshaker@uwaterloo.ca).

Digital Object Identifier 10.1109/JSEN.2022.3184188

Most of the current radar-based gait assessments were conducted in large clutter-free environments [6], [7], [26]–[28]. However, there is a pressing need to develop gait assessment solutions for naturalistic settings (e.g., individual's homes, long-term care, and hospitals). One of the main challenges in such environments is the existence of stationary objects (i.e., clutter), creating multipath or ghosting effects [1]. Multipath occurs when a signal takes two or more paths from the transmitting antenna to the receiving antenna. The number and particular behaviour of the multiple paths depends on the room structure and the presence of objects [1]. The multipath issue is more significant when people walk in the space since moving even a small object in an environment causes changes in multipath reflections [1]. To be clinically meaningful and broadly applicable, radar technologies must be able to work in practical settings where day-to-day gait assessments will be made.

An element of most living environments (including private homes, retirement homes, long-term care, and hospitals) is a corridor or hallway. This provides a physical location where people will walk in a relatively constrained and predictable way many times a day. Walls in the hallway have a strong "clutter" impact, creating multipath due to the wide beam of commercially available radar antennas. In our previous work [29], [30], we designed an in-package hyperbola-based dielectric lens antenna to sharpen the radar antenna's beam to mitigate the multipath problem. While the lens antenna could be a promising solution at high frequencies, it was exclusively designed for AWR1443Boost. Designing and fabricating a similar antenna for each radar sensor would be time-consuming and impractical. Hence, we turned our attention from hardware design to signal processing.

In this paper, we propose a novel hallway gait monitoring algorithm to address the multipath problem that could be deployed for any radar type without the need for radar sensor alteration or modification. Our proposed method uses the MIMO features of an FMCW radar to find the range and azimuth heatmap of the environment along with the Doppler information of the person who is walking. First, a density-based spatial clustering of applications with noise (DBSCAN) algorithm [31] is used to cluster detected points from 2D Constant False Alarm Rate (CFAR) detection [32]. Then, we propose a tracking algorithm to track the walking person over time while removing other "ghosting clusters" (i.e., clusters created due to multipath effects). While the hallway walls create strong reflections, this technique enables our hallway gait monitoring algorithm to only track the person walking. After finding the proper position of the subject in range and azimuth, another set of signal processing chains is performed to extract gait instance spatiotemporal values at each cycle.

Although radar sensors have been widely used for gait analysis, only gait speed was extracted [7], [25], [33], [34]. While walking speed is a good and important gait parameter, additional parameters are needed for a more complete prediction and assessment, such as fall risk assessment [35]. There are a number of existing studies that employ radar systems and extract several average gait parameters over the entire walking period [5], [26], [35], [36]. For example, in [36], two radar sensors and a treadmill were used to extract average spatiotemporal gait parameters. However, none have developed an automated approach and system that can extract gait parameters at each single gait cycle. Additionally, most of the existing studies used radar sensors for almost a clutter-free environment [26], [35], [36]. Therefore, in contrast to the existing published research, we employed only one single FMCW radar and developed autonomous algorithms for gait analysis and conducted experiments in a highly-cluttered environment. The accurate results shown in this paper are in the acceptable error range to be clinically meaningful [37]. Our main contributions to this paper are:

1. An innovative method to remove multipath signals and track the subject in such a cluttered environment in the hallway.
2. A novel algorithm to extract spatiotemporal gait parameters at each single gait cycle, such as speed, step points, step length, stride length and step count, using only one FMCW radar sensor.

The remainder of this paper describes the algorithm and presents preliminary testing of its accuracy and applicability.

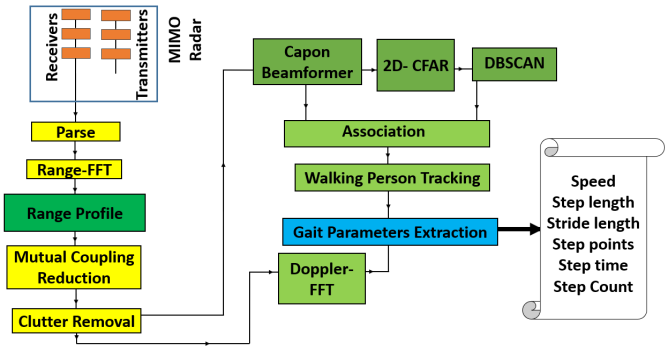

Fig. 1. Proposed hallway gait monitoring algorithm.

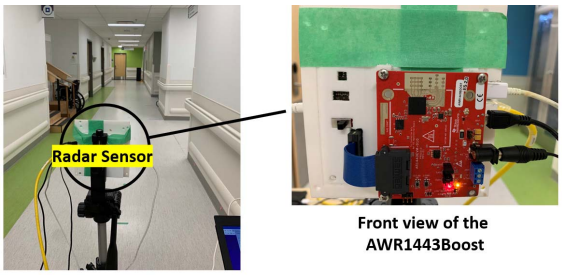

Fig. 2. Experimental setup for 14 m-hallway walk.

II. Hallway Gait Monitoring Algorithm

The block diagram of our proposed hallway gait monitoring algorithm is illustrated in Fig. 1. In order to show the detail of our proposed system and the corresponding result of each section of the algorithm, we provide the results of the proposed system deployed in a long hallway, pictured in Fig. 2. It should be noted that in the hallway alcove, there was a hospital transport stretcher, a wheelchair, a medical cart, a metal cabinet and some other wooden objects, causing too many multipath effects. We used a commercially available mm-wave FMCW radar (AWR1443Boost, available from Texas Instruments) operating at 77 GHz – 81 GHz [38]. It should be mentioned that our proposed algorithm could be paired with any other type of MIMO FMCW radar.

TABLE I
RADAR SENSOR AND PROPOSED GAIT EXTRACTION ALGORITHM'S PARAMETERS

Parameter	Description	Value
Start Frequency (GHz)	The frequency the radar signal will start at	77
Frequency Slope (MHz/μs)	The slope at which the frequency of the radar is increasing.	20
Idle time (μs)	The time between the previous chirp finishing and the frequency ramp starting	250
ADC Start Time (μs)	The time where the ADC starts sampling	10
ADC Samples	The number of samples the ADC takes	256
ADC Sample Rate (kbps)	The rate at which the ADC takes samples	4400
Ramp End Time (μs)	The time where the frequency ramps finished	105
Chirps/ Frame	The number of chirps per frame	256
Bandwidth (MHz)	The difference between the maximum and the minimum frequency	2070
P_fa	Desired probability of false alarm	5e-2
Guard_cell	Guard cells are placed adjacent to the cell under test with the purpose of preventing signal components from leaking into the training cell	3
Train_cell	Leading and lagging cells around the cell under test	6
ε	The radius of the circle to be created around each data point to check the density	2
min_points	the minimum number of data points required inside that circle for that data point to be classified as a Core point	5

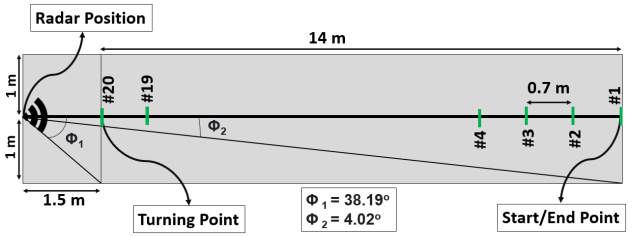

Fig. 3. Schematic of the hallway walking test setup. The green rectangles show the step points. The minimum and the maximum relative angle between the radar position and the hallway walls are θ_1 and θ_2, respectively.

As shown, the AWR1443Boost radar has four receivers (Rx) and three transmitters (Tx), giving it the capability to estimate both azimuth and elevation angles. Radar configuration along with a brief description of each parameter set for our experiment are listed in Table I. Since our goal was to cover 14 m walking segments, the radar was configured for a maximum range of 16.4986 m. The radar was placed 1.5 m away from the walking subject's starting point. The schematic of the hallway walking test setup is provided in Fig. 3. As shown, the maximum and minimum relative angle between the radar position and the hallway walls are 38.19° and 4.02°, respectively.

A. Parsing and Signal Processing

As shown in Fig. 1, the first step is parsing the received data collected from radar receivers. Since our signal processing methods are based on data captured from a MIMO FMCW radar, this provides the range, azimuth, and doppler information of the subject simultaneously [39]. In an FMCW radar, the first FFT (range-FFT) is performed to provide a range profile. Moreover, since transmitters and receivers are collocated in most commercially available MIMO radars, a mutual coupling reduction algorithm [39] is performed to remove the leakage between the transmitter and receiver.

B. Clutter Removal

The received signal includes not only the desired walking subject itself but also unwanted detections, known as clutter, which come from the reflections of, e.g., walls, floor, or objects around (i.e., passive clutter). A clutter removal algorithm is applied to remove such clutter signals [39]. To remove the reflections from the passive clutter, the average value of the signal is computed and subtracted from the aggregated signals. Since the signal variation reflected by clutter is small, removing the average is equivalent to eliminating the stationary scatter [39], [40]. Compared with passive clutter, humans have a much higher variation through their breathing, heartbeat, and small movements even when standing still, and thus this variation is more significant during walking. To show the effectiveness of the clutter removal algorithm in removing passive clutter and to ensure that signals coming from static objects are cleaned, Fig. 4 (a) shows the Short-Time Fourier-Transform (STFT) result [10], [39] of the hallway environment before performing the clutter removal algorithm when no subject was there. A strong strip around the zero Doppler (zero doppler represents the clutter in the STFT pattern [39]) with an amplitude of around 127 dB is visible, showing the richness of the reflections from the passive clutter. Fig. 4 (b) shows the same scenario but after clutter removal. As seen, the reflections from the passive clutter are removed, and there is no spot around zero doppler. From Fig 4 (a) and (b), we can conclude that the reflections from the passive clutter are removed by performing the clutter removal algorithm, and thus any remaining signals after performing the clutter removal algorithm is the result of the interactions between the subject walking in the hallway with the hallway environment (i.e., active clutter or multipath/ ghosting effects), but not from the passive clutter. More details of the clutter removal algorithm and its performance could be found in our previous works [10], [39].

The range-time map of the environment when a subject was walking across the hallway is provided in Fig. 5 after performing clutter removal. As shown, there are various reflections other than the direct reflections from the subject, created due to multipath reflections in such a cluttered environment. In most gait monitoring algorithms [6], [7], it is assumed that the maximum value of the range profile or of the STFT pattern represents the torso's bin [26], [40], [41]. However, as shown in Fig. 5 and 6, due to the multipath effects, isolating the

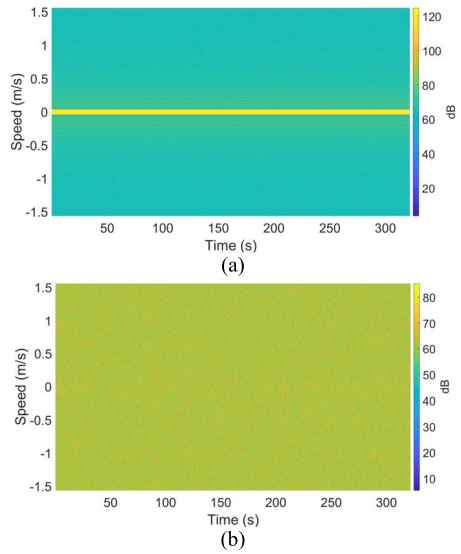

Fig. 4. STFT patterns of the hallway environment (a) before clutter removal without any subject and (b) after clutter removal without any subject.

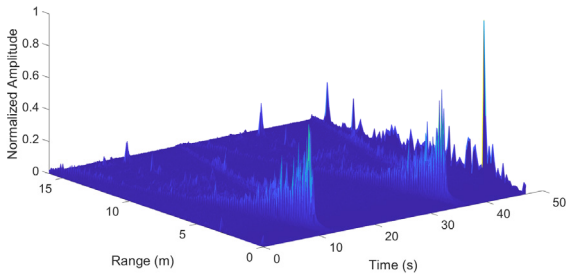

Fig. 5. Range-time map of the environment after performing clutter removal algorithm when the subject was walking across the hallway.

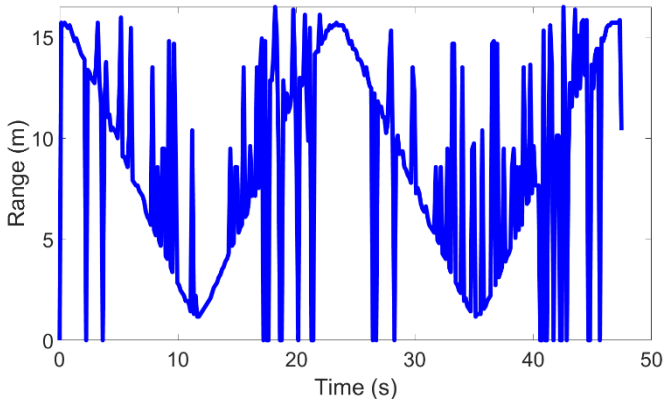

Fig. 6. Range of the walking subject over time obtained from the common gait extraction algorithm.

maximum values of the range bin would not result in obtaining the torso's correct position. This is because of the constructive and destructive feature of the electromagnetic waves, where the amplitude of the multipath signals could be larger than the direct reflection from the subject. Therefore, the torso's range bin cannot accurately be obtained by extracting the maximum amplitude from the range profile. The same limitation also applies to isolating maximum values from the STFT patterns.

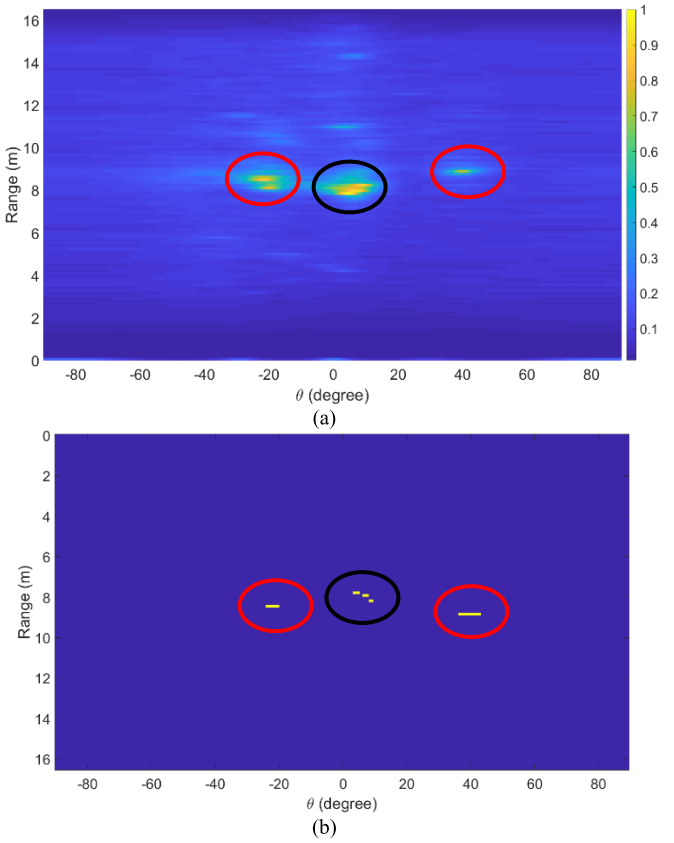

Fig. 7. A single frame example of the range-azimuth of a walking subject: (a) the Capon beamformer results (b) CFAR outputs at frame 122. The black circle represents the subject being tracked, and the red circles represent reflections.

To find the correct bin of the subject's torso, after generating a range profile of the subject and clutter removal, we performed a Capon beamformer algorithm to create a range-azimuth heatmap of the environment [42], [43]. This method not only paves the way for future versions of the algorithm that can track multiple subjects but provides more information on the environment to distinguish between the reflections from the walking subject and their multipath effects. We refer the reader to our previous publications for details regarding how we applied the Capon beamformer algorithm to create range-azimuth heatmaps of the environment [42]–[44].

C. 2D-CFAR

As shown in Fig. 7 (a), the range-azimuth heatmap represents the density of reflected signals in the environment. If a walking subject is at a specific range and azimuth, that location has more reflections in comparison with other non-occupied positions. This phenomenon is true if there are no multipath effects or the heatmap is obtained in a clutter-free environment. However, as shown in Fig. 7, in addition to the walking person's position (in the black circle), the heatmap also shows other strong reflections (in the red circles). The amplitude of the multipath signals is more than the subject's direct reflected signals.

Therefore, the position of the walking signals could not be isolated by taking the maximum values of the range-azimuth heatmap. Because the reflections from the hallway

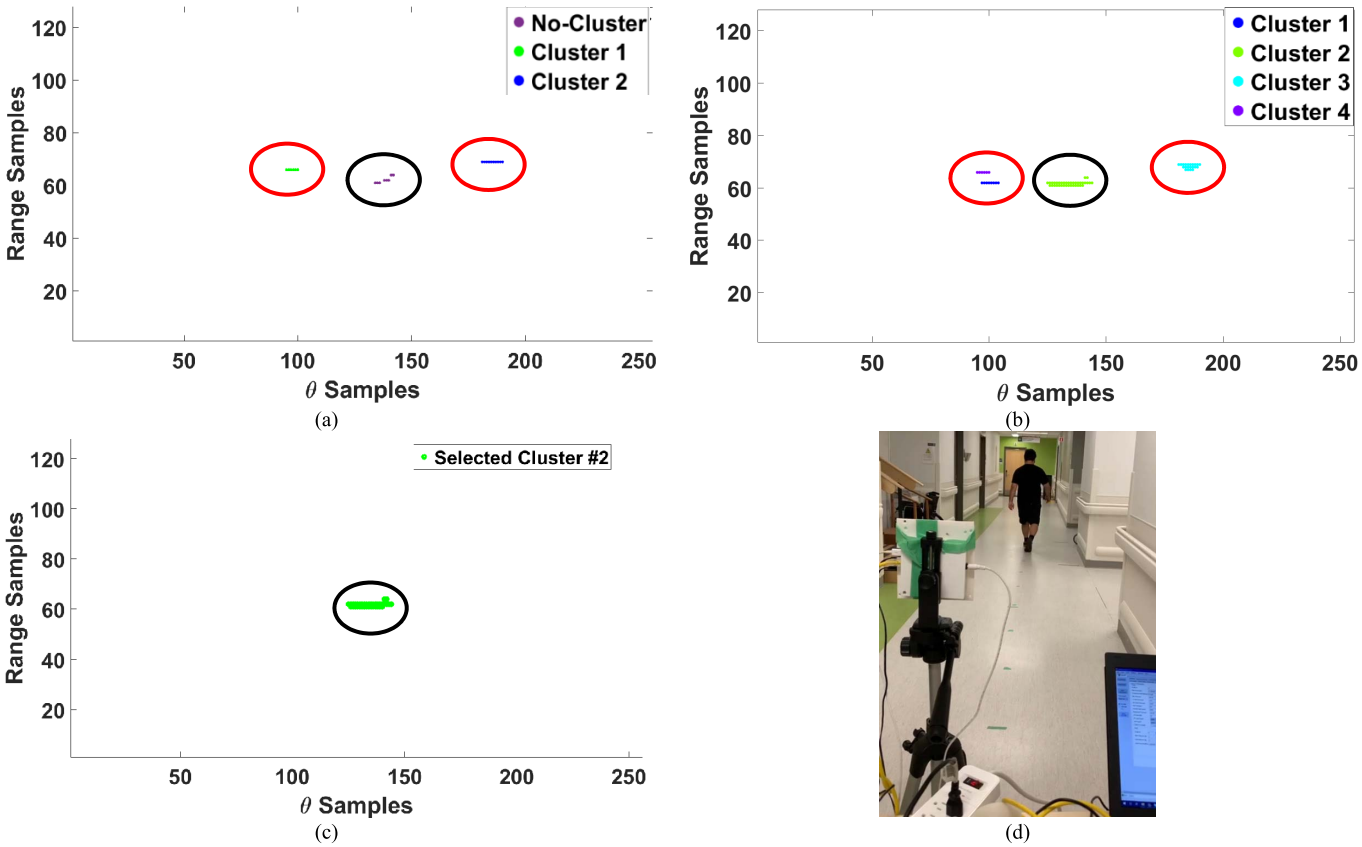

Fig. 8. Output of the DBSCAN algorithm at frame 122 (a) applied to the data from one frame, (b) applied to the aggregated frames, (c) target cluster among other ghosting clusters based on the tracking method; the black circle represents the subject being tracked, and the red circles represent ghosting clusters and (d) the corresponding snapshot of the video.

cause too much noise/anomalies, the common gait monitoring algorithm [5], [22], [36] could not accurately extract gait values in a highly cluttered environment, as shown in Fig. 6. Hence, an algorithm is required to find the exact position of the walking subject over time (to track the walking subject) before performing a gait extraction algorithm. To do so, we first perform 2D-CFAR [32] to detect signals and remove noise from the range-azimuth heatmap. Fig. 7 (b) shows the 2D-CFAR output of the subject's detected points and the ghosting effects.

D. Unsupervised Machine Learning: DBSCAN

To remove the ghosting clusters and to track the subject walking across the hallway, an unsupervised machine learning algorithm is applied to cluster the detected points. This allows for the separation and identification of the true signal from the ghosting ones. Since the multipath effects in our application vary from one frame to the other, sufficient information about the number of ghosting clusters is not known. As the density-based clustering does not require one to specify the number of clusters in the data a priori, we chose to apply the density-based spatial clustering of applications with noise (DBSCAN) algorithm to group the detected points [31].

For a point to be assigned to a cluster, it must satisfy the condition that its epsilon neighbourhood (ε) contains at least a minimum number of neighbours (*min_points*). Based on the performance of the different variables set for the DBSCAN parameters, $\varepsilon = 2$, and *min_points* $= 5$ were selected as optimized values. However, to reliably group the detected points from the walking subject to a correct cluster, we realized that data from one frame is not sufficient. As shown in Fig. 8 (a), the purple points (subjects detected points) are estimated as noise points or "No-Cluster"—an outlier that does not belong to any cluster. Note that each range sample represents 12.99 cm and each θ sample is 0.6990º. To prevent missed detection and to avoid having empty detected points as an input for the clustering algorithm, the clustering algorithm should be applied to the aggregated data over time. It has been shown in our previous radar-based human monitoring application research that adding time as an extra variable or having an observation time in the signal processing chain increases the accuracy of detection significantly (e.g., [39]. In other words, the subject being tracked might not appear in every single frame. Therefore, integrating multiple successive frames or detecting the subject over time can significantly improve detection accuracy. We, therefore, selected several frames (*N_frame* $= 3$) of range-azimuth heatmaps, aggregated their CFAR detected points, and then applied DBSCAN to the result. *N_frame* $= 3$ is selected to ensure the target cluster has enough detected points to satisfy the minimum clustering criteria. Additionally, it is chosen not to add too much complexity as the ghosting clusters would also be more if we aggregate more frames. As shown in Fig. 8 (b), by

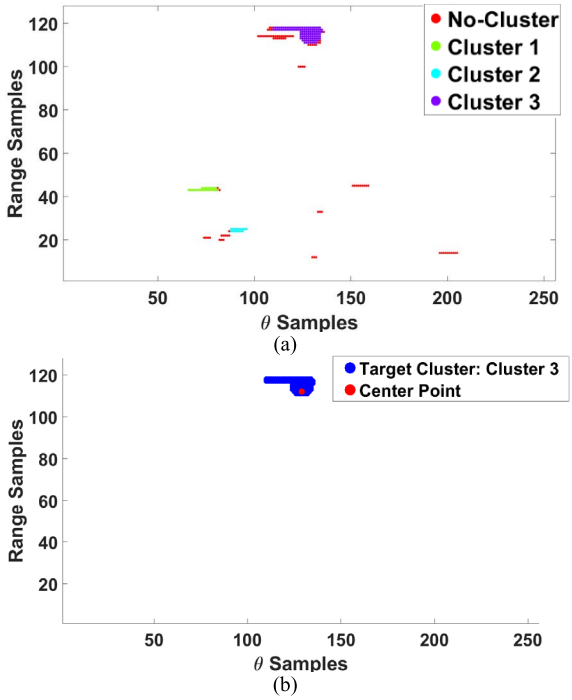

Fig. 9. Subject's initial position (a) detected clusters (b) target cluster (subject's cluster) and its center point to be tracked over time.

integrating the detected points over *N_frame* or equivalently adding time as an extra variable to the processing chain, the subject's detected points could be clustered correctly.

In order to remove ghosting clusters, associate the subject's cluster to its previous cluster and track the subject over time, we propose a tracking and association algorithm that identifies the subject's cluster (target cluster) during walking and associates it with the target cluster of the previous frame. Fig. 8 (c) demonstrates the target cluster obtained from our proposed tracking algorithms, detailed in the next subsection. Note that frame 122 in Fig. 8 helps to illustrate the detail in this paper, while the same results could be obtained in other frames. A screenshot of the video of the subject's walking process in frame 122 is provided in Fig. 8 (d). It should be mentioned that in this location of the hallway, there was a hospital transport stretcher and a medical cart on the right side of the subject in the hallway alcove.

E. Tracking and Association Algorithm

Our proposed tracking algorithm is shown in Algorithm 1.

1) Target Initial Position Extraction: To initiate the tracking and association process, we need to find the initial position of the subject that we wish to track. The initial position of the walking subject could be selected manually so that we can select the correct cluster that represents the subject from the DBSCAN outcome. For example, in Fig. 9(a), since the start position of the subject is known, we know that cluster 3 is the target cluster. However, as our goal is to have an autonomous system, it must be able to initiate the process accurately and automatically. We realized that for all initial points, the cluster with the maximum number of detected points is the subject's cluster. This fact is true only for the initial points when the subject is about to start walking as they were standing still and thus the same position for more than one frame. Therefore, the signal aggregation of almost the same position has more detected points than other positions. Additionally, as the subject is about to start walking and has less movement, the multipath reflections are comparatively less, while during the walking cycles, as will be shown in this paper, ghosting clusters could have more detected points. Thus, to get the initial position of the subject, the cluster with the maximum number of detected points was selected as the target cluster, as shown in Fig. 9 (b).

2) Subject Association/Tracking Over Time: Various radar tracking algorithms have been proposed and extensively used in different studies, such as extended Kalman filters, unscented Kalman filters (UKF), multiple hypothesis testing, particle filters and alpha-beta filter [45]–[48]. In a state-of-art processing pipeline, the radar detections from CFAR are passed into a tracking, for example, UKF, where track-to-detect association is done through detection gating, and the target state parameters (position and velocity) are updated by the tracker [49]. The velocity of the subject is an important decisive element in the aforementioned tracking methods, however, prediction based on the velocity of the subject might lead to inaccurate results. For example, if the subject is missed for a frame or due to the multipath effects, the target cluster is not selected correctly and thus, the velocity of the subject is obtained incorrectly for some frames, the prediction leads to inaccurate results. Moreover, the velocity of the subjects obtained from the Doppler highly depends on the relative angles between the subject and the radar, leading to an inaccurate outcome. In this paper, our main goal is to find the position of the subject and the subject's walking speed based on his position, but not his Doppler/velocity. Therefore, we base our tracking method on the current and previous positions of the subject, a point with the maximum amplitude of each cluster from the range-azimuth heat map, and some facts about walking cycles. Because the walking cycles are identified through time-based deep learning in our previous work [10], it ensures that the subject is walking, and his position should change over time. We propose our tracking and association method based on the Euclidean distance between two consecutive center points of the subject's cluster. Our method does not require a detailed system model, and its low computational complexity ensures code realization even on a microcontroller or a Raspberry Pi.

In order to associate each identified cluster with the previous one and to track the subject over time, we first calculate the center point of each cluster. Our criteria to find the center point of each cluster is to find the point in the cluster with the maximum amplitude. As each cluster has a *range_index* and *azimuth_index*–(range samples and θ samples in plots in this paper), these can be used to obtain the corresponding cluster's amplitude from the range-azimuth heatmap. For our method, we consider the whole body of a human being to be a single point [5]. This assumption holds because an individual's torso constitutes a significant part of the reflected signals, which means the torso line can be selected from the occupied radar range bins by isolating the maximum signal from his cluster [6], [7]. The center point of the initial subject position is shown in Fig. 9 (b) as an example. Therefore, if we select the torso's range bin from the subject's cluster, we can reliably extract distinctive and informative features of gait parameters

from the velocity of the torso speeding up and slowing down during the swing phase of each leg [50].

As detailed in Algorithm 1, in order to find the subject's cluster among other ghosting clusters, our criteria is to find the nearest point to the previous center point of the target cluster (*center_old*). For each frame, the algorithm takes the center position of the previous target cluster and the aggregated output of the detected points from CFAR. The DBSCAN algorithm is then applied to cluster the detected points. In the next step, the center of each cluster is calculated by obtaining the maximum amplitude of the cluster in the range-azimuth heatmaps. The Euclidean distance between the center point of the current cluster (*cluster_center*) to *center_old* is then calculated. The cluster with the closest center point to center_old is associated with the subject's cluster, which indicates the subject's torso's position. Consequently, the successive center points of the subject's cluster over time show the subject's position during walking. Tracking the subject over time provides the trajectory of walking (range, azimuth, and Doppler information). Based on the trajectory of walking, gait parameters can be extracted by performing our proposed gait extraction algorithm, described in section II. F. As an example, the tracking algorithm's output of frames 124 and 126 are shown in Fig. 10 (a) and (b), respectively. As seen, the algorithm correctly identifies the subject's clusters and associates them to the previous corresponding frame.

Algorithm 1 Association Tracking Algorithm

Input: range-azimuth heatmaps, CFAR outputs, initial_center
Output: Center points of the walking subject
center_old = initial_center
For i = *N_frame+1*: number of frames:
CF_Sum=0
  For n = i–*N_frame:i*
   CF_Sum = CFAR outputs (n)+ CF_Sum
CFAR outputs (i) = *CF_Sum*
If~isempty
detect_clusters = DBSCAN (CFAR outputs(i))
   For j = 1: length (detect_clusters):
   center = max (range_azimuth_map (detect_clusters)))
   dist (j) = Euclidean_distance (*cluster_center*, *center_old*)
   center = min (dist)
   center_points (i) = center
else
center_points (i) = *center_old*

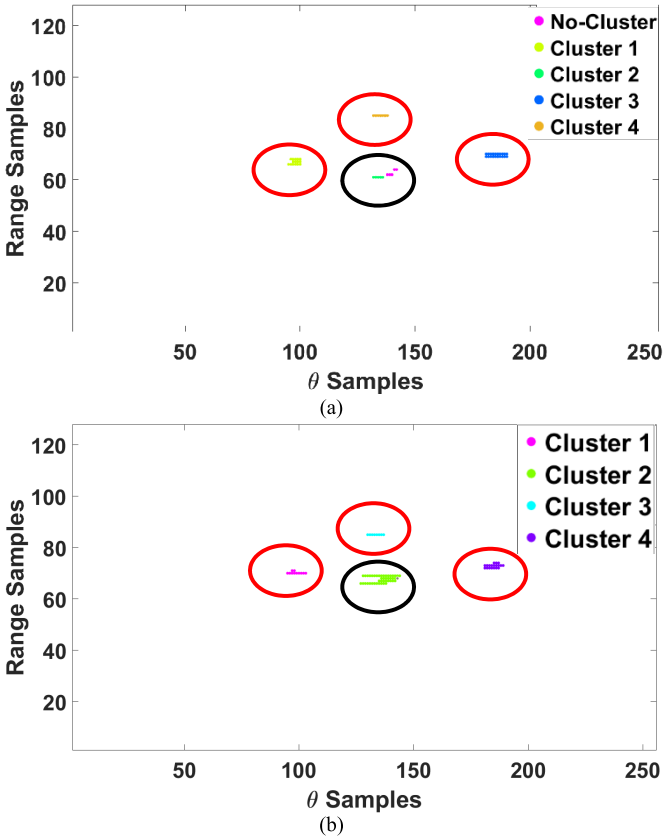

Fig. 10. Output of the DBSCAN and the tracking algorithm for (a) frame 124 and (b) frame 126. The black circle shows that the tracking algorithm correctly identified the cluster of data that corresponds to the true location of the subject.

F. Gait Extraction Algorithm

As shown in the diagram of our proposed gait extraction algorithm depicted in Fig. 11, using the position of the subject over time, the overall velocity of walking (i.e., the distance a walking person travels over a second (velocity = position/time)) can be calculated.

The velocity of the torso is calculated by performing a second FFT (Doppler-FFT) over the torso's range bin. Since the maximum velocity of the torso is achieved when the foot touches the ground (step time) [50], applying a peak detection algorithm to the results of the absolute value of Doppler-FFT over the torso's range bin, the torso's maximum speed is obtained. To extract the torso's maximum speed, a peak detection algorithm is applied to the Doppler-FFT. Based on the peak detection algorithm [51], a local peak is defined as a data sample which is either larger than the two neighbouring samples or is equal to infinity. We defined two variables for the peak detection algorithm, 'Min Peak Height' as MPH and 'Min Peak Distance' as MPD. MPH finds only those peaks that are greater than the minimum peak height, and MPD finds peaks separated by more than the minimum peak distance. MPD is specified to ignore smaller peaks that may occur in close proximity to a large local peak. In this paper, MPH is the minimum acceptable value of the maximum velocity of the torso. To find a proper value for the MPH, we assumed that the subject walks more than 0.5 m/s. Moreover, MPD is the minimum time interval between two consecutive step points. MPD is set to 0.1 s because we assumed that our subject could not take a step for less than 0.1 s. These two variables are selected based on the fact that our subjects are walking but not running. Moreover, several studies have shown that the cut-point for speed is 1 m/s [14], [15], meaning that any value less than this threshold might notify an unhealthy status of the subject. In this regard, we set MPH to 0.5 m/s to cover almost all types of subjects and even the worst-case scenarios when subjects walk very slowly. The corresponding time of the torso's maximum speed shows the time when the foot touches the ground (contact position time/step time). Then, the contact position time can be obtained, which can be used to determine

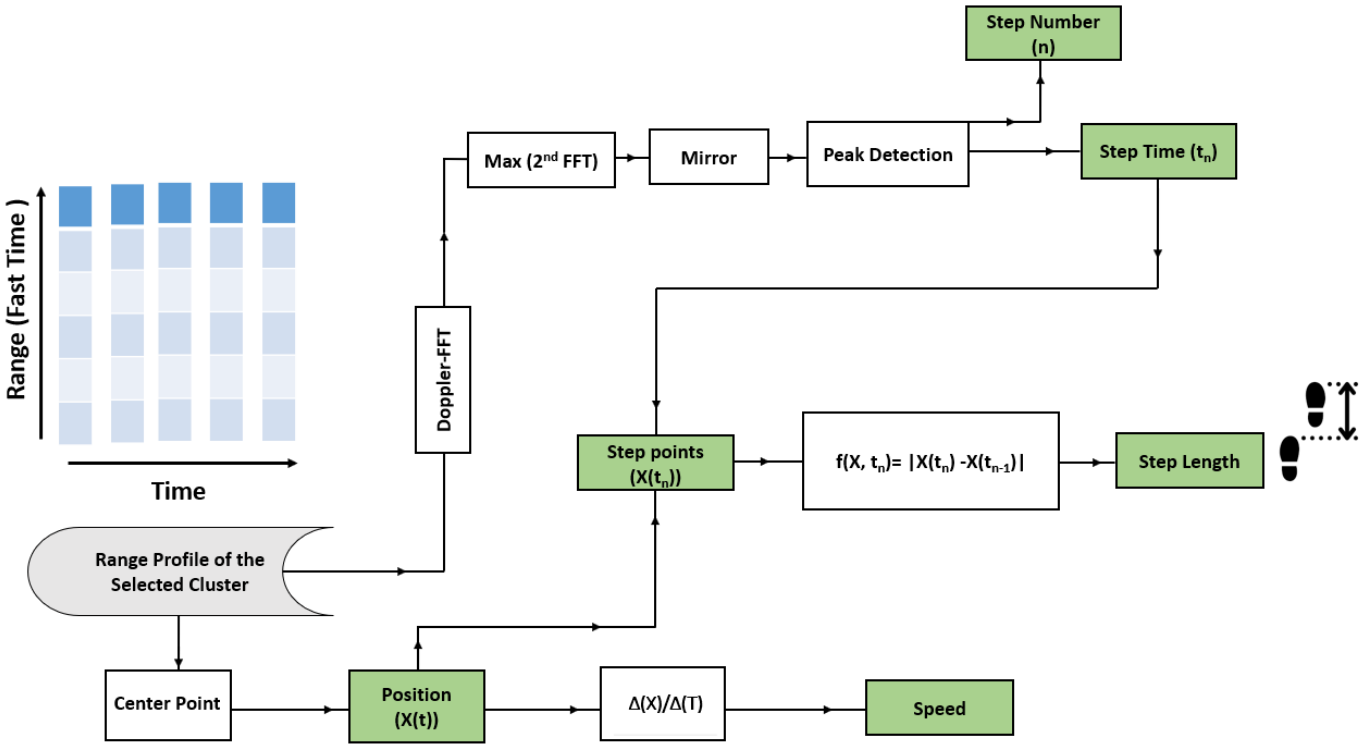

Fig. 11. Proposed gait parameter extraction algorithm.

the number of steps or step counts. Consequently, as shown in Fig. 11, knowing the step time of every single step (t_n) along with the position of the subject (X (t)), the step point of each step is acquired. The step length at each cycle is then obtained by subtracting two consecutive step points. Finally, a count of the number of occurrences of these maximum values over time results in the overall step count. It is worth mentioning that we take advantage of the distinctive feature of FMCW radars, providing the range and Doppler information of a subject simultaneously, enabling us to provide spatiotemporal gait parameters using only one radar sensor. While other methods reported in the literature have extracted the average value of cadence and other parameters by applying FFT on the spectrogram [36], [52]–[56], our proposed method can show the instance gait values (spatiotemporal gait parameters at every single gait cycle) of each metric. A full gait cycle is defined from one heel strike to the next [36]. The duration of a gait cycle is given by the stride time (or the duration of the two consecutive step times).

III. Experimental Results

The performance of the proposed system was evaluated in a long hallway pictured in Fig. 2. Gait parameters were extracted by asking five volunteers to walk back and forth along the hallway twice by following a straight line with marks showing the step points the volunteers were asked to step on. The total number of step points was 80 for the two full lapse walks. Although this setup might not properly represent normal gait, it gives a good estimate of the true gait without needing GaitRite or Vicon systems.

For all tests, comparison time values were recorded using a stopwatch and asking volunteers to follow a traced line, as depicted in Fig. 3. As shown in Fig. 13, the position and the time duration for the first 2 m-walk (T_1, R_1), the first 10 m-walk (|(T_2, R_2)-(T_1, R_1)|), the first turn (|(T_3, R_3)-(T_2, R_2)|), the second 10 m-walk (|(T4, R4)-(T3, R3)|), the second turn (|(T5, R_5)-(T_4, R_4)|), the third 10 m-walk (|(T_6, R_6)-(T_5, R_5)|), the third turn (|(T_6, R_6)-(T_7, R_7)|), the fourth 10 m-walk (|(T_8, R_8)-(T_7, R_7)|), the last 2 m-walk (|(T_{end}, R_{end})-(T_8, R_8)|) are calculated. Table II summarizes the gait values obtained using our proposed method along with the measured values. Note that the time it took for turning cycles (2 m-walk) is excluded in walking speed and step length calculation processes; therefore, 10 m-walk cycles were used for calculations. The "estimated values" in Table II are the number of steps the volunteers were asked to follow; thus, we assume our subjects followed the protocol perfectly. In order to demonstrate the performance of our proposed algorithm and to show the result of our gait extraction algorithm, we now present a case study of results from one of the volunteers. As shown in Fig. 12, having the position (range) of the subject while walking toward and away from the radar and corresponding time according to the protocol mentioned above, the average walking speed of 1.3618 m/s is calculated while the measured (stopwatch) value was 1.3699 m/s. Applying the Doppler-FFT to the torso's range bin, the velocity of the torso is obtained, as shown in Fig. 13.

Applying the peak detection algorithm to the absolute values of the velocity of the torso results in the identification of the step time of each gait cycle, step number, and step counts, as shown in Fig. 14. As the time of each step time is known

TABLE II
EXTRACTED GAIT PARAMETERS

Participant	Number of total steps (Estimated value: 80)	Number of 10 m-walk steps (Estimated value: 60)	Step length (cm) Estimated value (70 cm)	Speed Measured by our System (m/s)	Speed Measured by Stopwatch (m/s)
A	85	56	69.83	1.3765	1.3874
B	80	59	65.18	1.2811	1.2949
C	82	56	67.04	1.3734	1.4169
D	84	58	67.64	1.3618	1.3699
E	87	58	67.20	1.3281	1.3241
Average error for five participants	+3.6	-2.6	-2.622	0.0161 m/s	

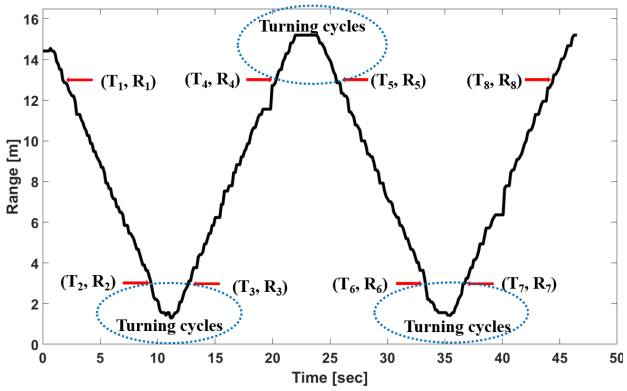

Fig. 12. Plot of walking speed captured by the radar system with points used for calculations indicated.

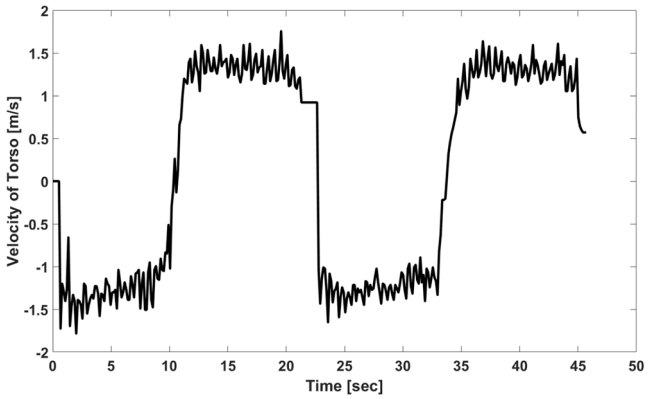

Fig. 13. Example of torso velocity during walking calculated by the radar system.

from Fig. 14, and the position of the person is obtained from Fig. 12, step points at each gait cycle can be obtained, as shown in Fig. 15. Step length can then be acquired by subtracting two successive step points, as shown in Fig. 15 by the red arrow and a photo of the step. This means that spatiotemporal gait parameters at each cycle, such as step points, step time, speed of torso, and step length, can be extracted in a long hallway using only one FMCW radar sensor.

As shown in Fig. 15, the total number of steps calculated by the system for the overall walk in our case study is 84, while the actual step number was 80. Correspondingly, as summarized in Table II, the average step length calculated by the system was 67.64 cm, while the distance marked on the floor was 70 cm.

The five subjects in this validation experiment have gait velocities that range from 1.2811 m/s to 1.3765 m/s, while the system's average absolute error for speed estimation ranged between 0.0040 m/s to 0.0435 m/s. The absolute error was obtained by comparing the speed results obtained from the radar sensor and a stopwatch. Although these results are preliminary (i.e., the small sample size in a constrained condition) and the 'ground truth' may have been flawed as it was recorded using a stopwatch, these results suggest our radar system may be accurate enough to detect clinically meaningful changes (i.e., changes on a scale of 0.05 m/s [37]. The step length of the individual subjects ranges from 65.18 cm to 69.83 cm, with an error of 0.17 cm to 4.82 cm, respectively. Additionally, the system had an average absolute error between 1 step to 4 steps in measuring step counts for 10 m-walk and 0 steps to 7 steps for the whole walking process. As shown, our proposed work is able to extract spatiotemporal gait values at each gait cycle using a single FMCW radar. It is also worth mentioning that, as shown in Fig. 14, step time, stride time and stance time could be extracted at each single gait cycle; however, as we did not have access to a GaitRite mat or a Vicon system, we did not report them in this paper.

In order to compare the outcomes of this paper with previous works, we listed a number of references in Table III with the reported error range, extracted gait parameters, the type of the radar and the number of radars used for their experiment. As shown, the error reported in our work is very low compared with other reported works, which is clinically meaningful [37]. Moreover, we used only one FMCW radar that provided both spatiotemporal gait parameters at each gait cycle, while other works either used two radars to provide some detailed gait parameters or added an extra device such as a treadmill to provide these parameters. Additionally, we provided spatiotemporal gait parameters at every single cycle; for instance, step time, step lengths, step points, etc., are extracted at each cycle for the first time in this paper. Therefore, while future work with a greater range of test conditions and more participants must be done to ascertain the accuracy of our algorithm, these preliminary results demonstrate the promising potential of our algorithm to accurately monitor several aspects of gait in hallways.

TABLE III
COMPARISON OF THE OUTCOMES OF THIS PAPER WITH OTHER PREVIOUS WORKS

Reference	Reported error for speed	Number of radars	Type of environment	Extracted parameters	Radar type and other required devices
[26]	Not reported	1	Low clutter	mean walking speed, maximum leg velocity, maximum leg velocity, mean leg velocity in swing and stance phase, degree of variation of leg velocity in swing and stance phase,	Micro-Doppler
[36]	For 1.1. m/s walk (foot velocity error): 0.06 m/s to 0.17 m/s	2	Low clutter	Stride time, stance time, flight time, step time, cadence, stride length, step length, maximal foot velocity, maximal ankle velocity, maximal knee velocity, time instant of maximal knee velocity:	Continuous waves and treadmill
[35]	0.144 m/s	2	Low clutter	Foot velocity, torso velocity, step time	pulse-doppler
[57]	For 10 GHz: slow walk: 0.4 m/s and normal walk: 0.14 m/s For 24 GHz: 0.5 m/s and normal walk: 0.06 m/s	1	Low clutter	Walking speed	10 GHz pulse-doppler 24 GHz FMCW
This work	0.0040 m/s to 0.0435 m/s	1	High clutter	At each gait cycle: walking speed, maximum velocity of the torso, step length, number of steps, step points, step time, step count	FMCW radar

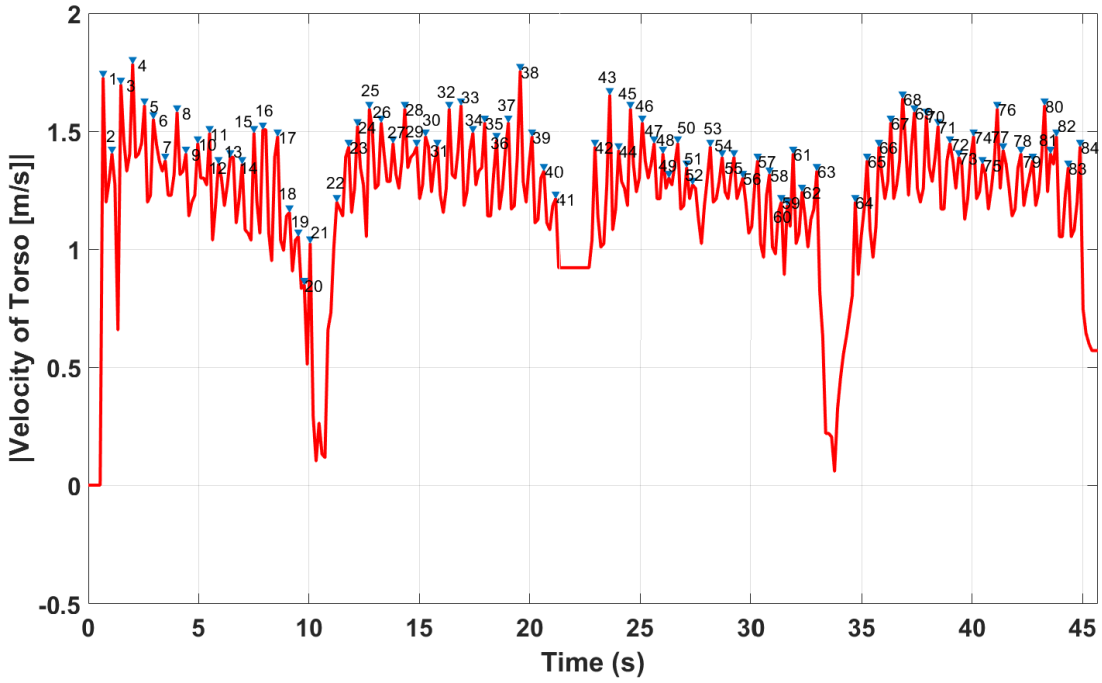

Fig. 14. Peak detection algorithm applied to the absolute value of the velocity of the torso. Step counts are shown by the small arrows and numbers above the velocity plot line.

It should be pointed out that as people in their natural environments might not start walking down hallways from standing still, to translate this approach to real-world applications, we need to add machine learning to the proposed signal processing chain to identify walking cycles and distinguish them from other activities. In this paper, we based our algorithm on the assumption that we know the subject is walking. However, in a real-world application, we first should identify

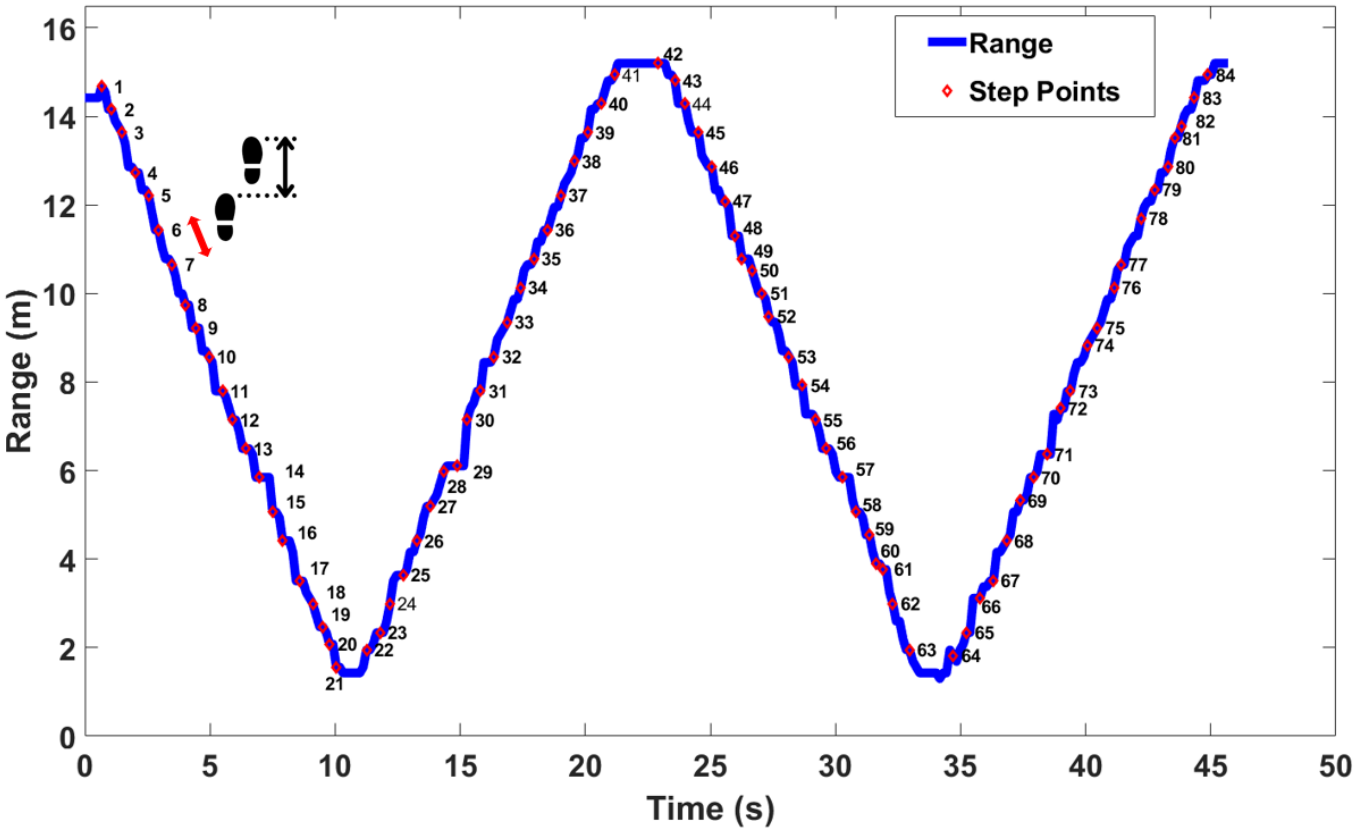

Fig. 15. Range of the person walking. Step points (dots) and step counts (numbers) detected by the algorithm are indicated on the plot line.

the walking cycles and then apply a gait monitoring algorithm. We refer interested readers to our previous work, where we used a sequential deep learning algorithm to identify walking cycles, distinguish them from other in-place movements, and recognize the type of activities [10].

IV. Conclusion

This paper proposes a novel method to extract an individual's gait parameters in a long hallway using a single FMCW radar. Preliminary validation testing of our system demonstrated unsupervised machine learning combined with our proposed tracking algorithm was able to track and monitor a walking subject in a cluttered environment such as a long hallway and extract spatiotemporal gait parameters. The relative simplicity and cost-effectiveness of this method make it a realistic approach to monitoring gait in real-world settings, including people's homes. Future work should focus on multiple gait monitoring scenarios.

References

[1] M. Mercuri *et al.*, "Enabling robust radar-based localization and vital signs monitoring in multipath propagation environments," *IEEE Trans. Biomed. Eng.*, vol. 68, no. 11, pp. 3228–3240, Nov. 2021, doi: 10.1109/TBME.2021.3066876.

[2] M. Alizadeh, G. Shaker, J. C. M. De Almeida, P. P. Morita, and S. Safavi-Naeini, "Remote monitoring of human vital signs using mm-Wave FMCW radar," *IEEE Access*, vol. 7, pp. 54958–54968, 2019, doi: 10.1109/ACCESS.2019.2912956.

[3] J.-Y. Kim, J.-H. Park, S.-Y. Jang, and J.-R. Yang, "Peak detection algorithm for vital sign detection using Doppler radar sensors," *Sensors*, vol. 19, no. 7, pp. 1–15, 2019, doi: 10.3390/s19071575.

[4] P. van Dorp and F. C. A. Groen, "Human walking estimation with radar," *IEE Proc., Radar, Sonar Navigat.*, vol. 150, no. 5, pp. 356–366, 2003, doi: 10.1049/ip-rsn:20030568.

[5] C.-Y. Hsu, Y. Liu, Z. Kabelac, R. Hristov, D. Katabi, and C. Liu, "Extracting gait velocity and stride length from surrounding radio signals," in *Proc. CHI Conf. Hum. Factors Comput. Syst.*, May 2017, pp. 2116–2126, doi: 10.1145/3025453.3025937.

[6] H. Abedi, G. Shaker, J. Boger, P. Morita, and A. Wong, "Use of millimeter wave FMCW radar to capture gait parameters," *Amer. J. Biomed. Sci. Res.*, vol. 6, no. 2, pp. 122–123, 2019, doi: 10.34297/AJBSR.2019.06.001009.

[7] A. Boroomand, G. Shaker, P. P. Morita, A. Wong, and J. Boger, "Autonomous gait speed estimation using 24 GHz FMCW radar technology," in *Proc. IEEE EMBS Int. Conf. Biomed. Health Informat. (BHI)*, Mar. 2018, pp. 66–69, doi: 10.1109/BHI.2018.8333371.

[8] D. Alshamaa, A. Chkeir, R. Soubra, and F. Mourad-Chehade, "Measurement of gait speed using a Doppler radar: Influence of acceleration and deceleration zones," in *Proc. IEEE Sensors Appl. Symp. (SAS)*, Mar. 2019, pp. 1–5, doi: 10.1109/SAS.2019.8706123.

[9] O. Postolache, J. M. D. Pereira, V. Viegas, and P. S. Girao, "Gait rehabilitation assessment based on microwave Doppler radars embedded in Walkers," in *Proc. IEEE Int. Symp. Med. Meas. Appl. (MeMeA) Proc.*, May 2015, pp. 208–213, doi: 10.1109/MeMeA.2015.7145200.

[10] H. Abedi, A. Ansariyan, P. P. Morita, J. Boger, A. Wong, and G. Shaker, "Sequential deep learning for in-home activity monitoring using mm-wave FMCW radar," in *Proc. IEEE Int. Symp. Antennas Propag. USNC-URSI Radio Sci. Meeting*, Dec. 2022, pp. 1499–1500, doi: 10.1109/APS/URSI47566.2021.9704291.

[11] J. Verghese, C. Wang, R. B. Lipton, R. Holtzer, and X. Xue, "Quantitative gait dysfunction and risk of cognitive decline and dementia," *J. Neurol. Neurosurg. Psychiatry*, vol. 78, no. 9, pp. 929–935, Sep. 2007, doi: 10.1136/jnnp.2006.106914.

[12] A. Alfaro-Acha, S. A. Snih, M. A. Raji, K. S. Markides, and K. J. Ottenbacher, "Does 8-foot walk time predict cognitive decline in older Mexicans Americans?" *J. Amer. Geriatrics Soc.*, vol. 55, no. 2, pp. 245–251, Feb. 2007, doi: 10.1111/j.1532-5415.2007.01039.x.

[13] G. A. van Kan *et al.*, "Gait speed, body composition, and dementia. The EPIDOS-Toulouse cohort," *J. Gerontol. A, Biol. Sci. Med. Sci.*, vol. 67, no. 4, pp. 425–432, Apr. 2012, doi: 10.1093/gerona/glr177.

[14] A.-K. Welmer, D. Rizzuto, C. Qiu, B. Caracciolo, and E. J. Laukka, "Walking speed, processing speed, and dementia: A population-based longitudinal study," *J. Gerontol. A, Biol. Sci. Med. Sci.*, vol. 69, no. 12, pp. 1503–1510, Dec. 2014, doi: 10.1093/gerona/glu047.

[15] R. A. Hackett, H. Davies-Kershaw, D. Cadar, M. Orrell, and A. Steptoe, "Walking speed, cognitive function, and dementia risk in the English longitudinal study of ageing," *J. Amer. Geriatrics Soc.*, vol. 66, no. 9, pp. 1670–1675, Mar. 2018, doi: 10.1111/jgs.15312.

[16] A. L. McDonough, M. Batavia, F. C. Chen, S. Kwon, and J. Ziai, "The validity and reliability of the GAITRite system's measurements: A preliminary evaluation," *Arch. Phys. Med. Rehabil.*, vol. 82, no. 3, pp. 419–425, Mar. 2001, doi: 10.1053/apmr.2001.19778.

[17] K. E. Webster, J. E. Wittwer, and J. A. Feller, "Validity of the GAITRite walkway system for the measurement of averaged and individual step parameters of gait," *Gait Posture*, vol. 22, no. 4, pp. 317–321, Dec. 2005, doi: 10.1016/j.gaitpost.2004.10.005.

[18] B. Bilney, M. Morris, and K. Webster, "Concurrent related validity of the GAITRite walkway system for quantification of the spatial and temporal parameters of gait," *Gait Posture*, vol. 17, no. 1, pp. 68–74, Feb. 2003, doi: 10.1016/S0966-6362(02)00053-X.

[19] A. Pfister, A. M. West, S. Bronner, and J. A. Noah, "Comparative abilities of Microsoft Kinect and Vicon 3D motion capture for gait analysis," *J. Med. Eng. Technol.*, vol. 38, no. 5, pp. 274–280, Jul. 2014, doi: 10.3109/03091902.2014.909540.

[20] B. G. Contini *et al.*, "A wearable gait analysis protocol to support the choice of the appropriate ankle-foot orthosis: A comparative assessment in children with cerebral palsy," *Clin. Biomech.*, vol. 70, pp. 177–185, Dec. 2019.

[21] *Physilog | Inertial Measurement Sensor (IMU)*. Accessed: Feb. 15, 2022. [Online]. Available: https://research.gaitup.com/physilog/

[22] K. Saho, K. Shioiri, M. Fujimoto, and Y. Kobayashi, "Micro-Doppler radar gait measurement to detect age- and fall risk-related differences in gait: A simulation study on comparison of deep learning and gait parameter-based approaches," *IEEE Access*, vol. 9, pp. 18518–18526, 2021, doi: 10.1109/ACCESS.2021.3053298.

[23] R. G. Raj, V. C. Chen, and R. Lipps, "Analysis of radar human gait signatures," *IET Signal Process*, vol. 4, no. 3, pp. 234–244, Mar. 2010, doi: 10.1049/iet-spr.2009.0072.

[24] J. Zhang, "Basic gait analysis based on continuous wave radar," *Gait Posture*, vol. 36, no. 4, pp. 667–671, Sep. 2012, doi: 10.1016/j.gaitpost.2012.04.020.

[25] B. Lau, S. Haider, A. Boroomand, G. Shaker, J. Boger, and P. Morita, "Gait speed tracking system using UWB radar," in *Proc. IET Conf. Publications*, 2018, pp. 4–7, doi: 10.1049/cp.2018.1258.

[26] K. Saho, K. Uemura, K. Sugano, and M. Matsumoto, "Using micro-Doppler radar to measure gait features associated with cognitive functions in elderly adults," *IEEE Access*, vol. 7, pp. 24122–24131, 2019, doi: 10.1109/ACCESS.2019.2900303.

[27] P. Addabbo, M. L. Bernardi, F. Biondi, M. Cimitile, C. Clemente, and D. Orlando, "Temporal convolutional neural networks for radar micro-Doppler based gait recognition," *Sensors*, vol. 21, no. 2, pp. 1–15, 2021, doi: 10.3390/s21020381.

[28] F. Quaiyum, N. Tran, J. E. Piou, O. Kilic, and A. E. Fathy, "Noncontact human gait analysis and limb joint tracking using Doppler radar," *IEEE J. Electromagn., RF. Microw. Med. Biol.*, vol. 3, no. 1, pp. 61–70, Mar. 2019, doi: 10.1109/JERM.2018.2881238.

[29] H. Abedi, P. P. Morita, J. Boger, A. Wong, and G. Shaker, "In-package integrated dielectric lens paired with a MIMO mm-wave radar for corridor gait monitoring," in *Proc. IEEE Int. Symp. Antennas Propag. USNC-URSI Radio Sci. Meeting (APS/URSI)*, Dec. 2021, pp. 1795–1796, doi: 10.1109/APS/URSI47566.2021.9704192.

[30] H. Abedi and G. Shaker, "Low-cost 3D printed dielectric hyperbolic lens antenna for beam focusing and steering of a 79 GHz MIMO radar," in *Proc. IEEE Int. Symp. Antennas Propag. North Amer. Radio Sci. Meeting*, Jul. 2020, pp. 1543–1544, doi: 10.1109/IEEECONF35879.2020.9329969.

[31] *DBSCAN Clustering Algorithm in Machine Learning—KDnuggets*. Accessed: Feb. 15, 2022. [Online]. Available: https://www.kdnuggets.com/2020/04/dbscan-clustering-algorithm-machine-learning.html

[32] *Constant False Alarm Rate (CFAR) Detection—MATLAB & Simulink*. Accessed: Mar. 6, 2022. [Online]. Available: https://www.mathworks.com/help/phased/ug/constant-false-alarm-rate-cfar-detection.html

[33] A. N. Aicha, G. Englebienne, and B. Kröse, "Continuous measuring of the indoor walking speed of older adults living alone," *J. Ambient Intell. Hum. Comput.*, vol. 9, no. 3, pp. 589–599, Jun. 2018, doi: 10.1007/s12652-017-0456-x.

[34] P. E. Cuddihy *et al.*, "Radar walking speed measurements of seniors in their apartments: Technology for fall prevention," in *Proc. Annu. Int. Conf. IEEE Eng. Med. Biol. Soc. (EMBS)*, Aug. 2012, pp. 260–263, doi: 10.1109/EMBC.2012.6345919.

[35] F. Wang, M. Skubic, M. Rantz, and P. E. Cuddihy, "Quantitative gait measurement with pulse-Doppler radar for passive in-home gait assessment," *IEEE Trans. Biomed. Eng.*, vol. 61, no. 9, pp. 2434–2443, Sep. 2014, doi: 10.1109/TBME.2014.2319333.

[36] A.-K. Seifert, M. Grimmer, and A. M. Zoubir, "Doppler radar for the extraction of biomechanical parameters in gait analysis," *IEEE J. Biomed. Health Informat.*, vol. 25, no. 2, pp. 547–558, Feb. 2021, doi: 10.1109/JBHI.2020.2994471.

[37] S. Perera, S. H. M. PharmD, R. C. Woodman, and S. A. Studenski, "Meaningful change and responsiveness in common physical performance measures in older adults," *J. Amer. Geriatrics Soc.*, vol. 54, no. 5, pp. 743–749, May 2006, doi: 10.1111/J.1532-5415.2006.00701.X.

[38] *AWR1443 Data Sheet, Product Information and Support*. Accessed: Aug. 12, 2021. [Online]. Available: https://www.ti.com/product/AWR1443

[39] H. Abedi, C. Magnier, V. Mazumdar, and G. Shaker, "Improving passenger safety in cars using novel radar signal processing," *Eng. Rep.*, vol. 3, no. 12, Dec. 2021, Art. no. e12413, doi: 10.1002/ENG2.12413.

[40] K. Saho, M. Fujimoto, M. Masugi, and L.-S. Chou, "Gait classification of young adults, elderly non-fallers, and elderly fallers using micro-Doppler radar signals: Simulation study," *IEEE Sensors J.*, vol. 17, no. 8, pp. 2320–2321, Apr. 2017, doi: 10.1109/jsen.2017.2678484.

[41] K. Saho, K. Uemura, and M. Matsumoto, "Remote assessment of gait deterioration due to memory impairment in elderly adults using micro-Doppler radar," in *Proc. IEEE 18th Int. Conf. Bioinf. Bioeng. (BIBE)*, Oct. 2018, pp. 181–184, doi: 10.1109/BIBE.2018.00042.

[42] H. Abedi, S. Luo, V. Mazumdar, M. M. Y. R. Riad, and G. Shaker, "AI-powered in-vehicle passenger monitoring using low-cost mm-wave radar," *IEEE Access*, vol. 10, pp. 18998–19012, 2022, doi: 10.1109/ACCESS.2021.3138051.

[43] M. Alizadeh, H. Abedi, and G. Shaker, "Low-cost low-power in-vehicle occupant detection with mm-wave FMCW radar," *Proc. IEEE Sensors*, Oct. 2019, pp. 1–4, doi: 10.1109/SENSORS43011.2019.8956880.

[44] H. Abedi, S. Luo, and G. Shaker, "On the use of low-cost radars and machine learning for in-vehicle passenger monitoring," in *Proc. IEEE 20th Top. Meeting Silicon Monolithic Integr. Circuits RF Syst. (SiRF)*, Jan. 2020, pp. 63–65, doi: 10.1109/SIRF46766.2020.9040191.

[45] E. Cortina, D. Otero, and C. E. D'Attellis, "Maneuvering target tracking using extended Kalman filter," *IEEE Trans. Aerosp. Electron. Syst.*, vol. 27, no. 1, pp. 155–158, Jan. 1991, doi: 10.1109/7.68158.

[46] S. Chang, N. Mitsumoto, and J. W. Burdick, "An algorithm for UWB radar-based human detection," in *Proc. IEEE Radar Conf.*, May 2009, pp. 1–6, doi: 10.1109/RADAR.2009.4976999.

[47] J. Zhang, T. Jin, Y. He, L. Qiu, and Z. Zhou, "Human tracking using range and velocity measurements by multistatic radar," in *Proc. Prog. Electromagn. Res. Symp. (PIERS)*, 2016, pp. 520–525, doi: 10.1109/PIERS.2016.7734384.

[48] C. Will, P. Vaishnav, A. Chakraborty, and A. Santra, "Human target detection, tracking, and classification using 24-GHz FMCW radar," *IEEE Sensors J.*, vol. 19, no. 17, pp. 7283–7299, Sep. 2019, doi: 10.1109/JSEN.2019.2914365.

[49] P. Vaishnav and A. Santra, "Continuous human activity classification with unscented Kalman filter tracking using FMCW radar," *IEEE Sensors Lett.*, vol. 4, no. 5, pp. 1–4, May 2020, doi: 10.1109/LSENS.2020.2991367.

[50] C. Hornsteiner and J. Detlefsen, "Characterisation of human gait using a continuous-wave radar at 24 GHz," *Adv. Radio Sci.*, vol. 6, pp. 67–70, May 2008, doi: 10.5194/ARS-6-67-2008.

[51] *Peak Analysis—MATLAB & Simulink Example*. Accessed: May 20, 2022. [Online]. Available: https://www.mathworks.com/help/signal/ug/peak-analysis.html;jsessionid=8073d5f14c99d3ea8a8919bee82c

[52] T. Yardibi *et al.*, "Gait characterization via pulse-Doppler radar," in *Proc. IEEE Int. Conf. Pervasive Comput. Commun. Workshops (PERCOM Workshops)*, Mar. 2011, pp. 662–667, doi: 10.1109/PERCOMW.2011.5766971.

[53] A.-K. Seifert, A. M. Zoubir, and M. G. Amin, "Detection of gait asymmetry using indoor Doppler radar," in *Proc. IEEE Radar Conf. (RadarConf)*, Apr. 2019, pp. 1–6, doi: 10.1109/RADAR.2019.8835611.

[54] L. Fei, H. Binke, Z. Hang, and D. Hao, "Human gait recognition using micro-Doppler features," in *Proc. 5th Global Symp. Millim.-Waves (GSMM)*, May 2012, pp. 326–329, doi: 10.1109/GSMM.2012.6314067.
[55] J. W. Palmer, K. F. Bing, A. C. Sharma, and J. B. Perkins, "Exploitation of radar Doppler signatures for gait analysis," in *Proc. Conf. Rec. 46th Asilomar Conf. Signals, Syst. Comput. (ASILOMAR)*, Nov. 2012, pp. 629–632, doi: 10.1109/ACSSC.2012.6489085.
[56] D. Boutte, V. R. Radzicki, M. Gumley, S. Hunt, P. Taylor, and A. Hunt, "A multistatic Doppler radar system with application to aeroecology," in *Proc. IEEE Radar Conf. (RadarConf)*, May 2017, pp. 47–51, doi: 10.1109/RADAR.2017.7944169.
[57] P. P. Morita *et al.*, "Comparison of gait speed estimation of multiple sensor-based technologies," in *Proc. Int. Symp. Hum. Factors Ergonom. Health Care*, Sep. 2019, vol. 8, no. 1, pp. 135–139, doi: 10.1177/2327857919081032.

Hajar Abedi (Graduate Student Member, IEEE) received the B.Sc. and M.Sc. degrees in electrical engineering from the Babol Noshirvani University of Technology, Babol, Iran, in 2014 and 2017, respectively. She is pursuing the Ph.D. degree with the Systems Design Engineering Department, University of Waterloo. Her research interests include antenna design, radar sensors, signal processing, and machine learning.

Jennifer Boger (Member, IEEE) team with the Intelligent Technologies for Wellness and Independent Living Laboratory (www.itwil.ca) engages in transdisciplinary collaboration and human-centric design practices that blend state-of-the art knowledge from computer science, engineering, and health sciences to create internationally renowned intelligent assistive technologies for supporting graceful aging. Dr. Boger's research focuses on creating technologies that enable more inclusive, equitable, and personal support for health, wellbeing, and quality of life for older adults.

Plinio P. Morita (Member, IEEE) is a Leading Researcher in the use of AI and IoT for public health and global health initiatives. At the UbiLaboratory, his research team focuses on the use of big data and AI to improve current public health surveillance mechanisms and support countries in the monitoring of health indicators (e.g., physical activity, sleep, and sedentary behavior), and environmental factors (e.g., heatwaves and extreme air pollution). Prof. Morita's research team has developed large-scale data collection ecosystems for supporting local initiatives in Canada and low and middle income countries (LMIC) in their efforts to better understand the impact of the COVID-19 pandemic on health behaviors, the impact of extreme air pollution on child and maternal health in LMICs (in partnership with UNICEF Mongolia), and the impact of heatwaves on seniors around the globe (in partnership with Health Canada and the Public Health Agency of Canada).

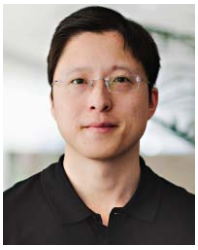

Alexander Wong (Senior Member, IEEE) is currently the Canada Research Chair of Artificial Intelligence and Medical Imaging, a member of the College of the Royal Society of Canada, the Co-Director of the Vision and Image Processing Research Group, and a Professor with the Department of Systems Design Engineering, University of Waterloo. He has published over 600 refereed journals and conference papers, and patents, in various fields such as computational imaging, artificial intelligence, computer vision, and multimedia systems. He has received numerous awards, including three outstanding performance awards, a Distinguished Performance Award, an Engineering Research Excellence Award, a Sandford Fleming Teaching Excellence Award, an Early Researcher Award from the Ministry of Economic Development and Innovation, a Best Paper Award at the NIPS Workshop on NIPS Workshop on Transparent and Interpretable Machine Learning in 2017, a Best Paper Award at the NIPS Workshop on Efficient Methods for Deep Neural Networks in 2016, an Outstanding Paper Award at the CVPR Workshop on Adversarial Machine Learning in Real-World Computer Vision Systems and Online Challenges in 2021, two best paper awards by the Canadian Image Processing and Pattern Recognition Society (CIPPRS) in 2009 and 2014, a Distinguished Paper Award by the Society of Information Display in 2015, three best paper awards for the Conference of Computer Vision and Imaging Systems (CVIS) in 2015, 2017, and 2018, Synaptive Best Medical Imaging Paper Award in 2016, two Magna Cum Laude Awards, and one Cum Laude Award from the Annual Meeting of the Imaging Network of Ontario, and the Alumni Gold Medal.

George Shaker (Senior Member, IEEE) is the Laboratory Director of the Wireless Sensors and Devices Laboratory, University of Waterloo-Schlegel Research Institute for Aging, where he is also an Adjunct Professor with the Department of Electrical and Computer Engineering and the Research Professor with the Department of Mechanical and Mechatronics Engineering. He is also with the Centre for Intelligent Antenna and Radio Systems (CIARS), University of Waterloo, Centre for Bioengineering and Biotechnology (CBB), and the Waterloo Centre for Automotive Research (WatCAR). Previously, he was an NSERC Scholar with the Georgia Institute of Technology. He also held multiple roles with RIM's (BlackBerry). With more than ten years of industrial experience in technology, and about six years as a Faculty Member leading project related to the application of wireless sensor systems for healthcare, automotives, and unmanned aerial vehicles, Prof. Shaker has many design contributions in commercial products available from startups and established companies alike. A sample list includes Google, COM DEV, Honeywell, Blackberry, Konka, DBJ, Enice, Spark Tech Laboratory, China Mobile, TriL, Bionym, Lyngsoe Systems, ON Semiconductors, Ecobee, Medella Health, NERV Technologies, Novela, Thalmic Labs, North, General Dynamics Land Systems, General Motors, Toyota, Maple Lodge Farms, Rogers Communications, and Purolator. He has authored/coauthored more than more than 80 publications and more than 30 patents/patent applications. He has received multiple recognitions and awards, including the IEEE AP-S Best Paper Award (the IEEE AP-S Honorable Mention Best Paper Award (four times to-date), the IEEE Antennas and Propagation Graduate Research Award (the IEEE MTT-S Graduate Fellowship, the Electronic Components and Technology Best of Session Paper Award, and the IEEE Sensors Most Popular Paper Award. He coauthored two papers in IEEE journals were among the top 25 downloaded papers on IEEEXplore for several consecutive months. He was the Supervisor of the student team winning the third best design contest at IEEE AP-S 2016, the coauthor of the ACM MobileHCI 2017 Best Workshop Paper Award, and the 2018 Computer Vision Conference Imaging Best Paper Award. He co-received with his students several research recognitions, including the NSERC Top Science Research Award 2019, IEEE APS HM Paper Award 2019, Biotec Top Demo Award 2019, arXiv top downloaded paper (medical device category) 2019, Velocity fund 2020, NASA Tech Briefs HM Award (medical device category) 2020, UW Concept Winner 2021, U.K. Dragons Canadian Competition Winner 2021, CMC Nano Winner 2021, and a Google Research Award 2021.